New Journal of Physics
The open-access journal for physics

Surface alloying of thin beryllium films on tungsten

A Wiltner and Ch Linsmeier[1]
Max-Planck-Institut für Plasmaphysik, EURATOM Association,
Boltzmannstr. 2, D-85748 Garching b. München, Germany
E-mail: linsmeier@ipp.mpg.de

New Journal of Physics **8** (2006) 181
Received 2 May 2006
Published 8 September 2006
Online at http://www.njp.org/
doi:10.1088/1367-2630/8/9/181

Abstract. The bimetallic system Be–W is studied after room temperature deposition of Be films on W and annealing experiments up to 1070 K using x-ray photoelectron spectroscopy (XPS). Already at room temperature an intermixing at the interface occurs. The amount of intermetallic compound increases during the annealing experiments, but is limited to ∼1.2 nm. The surface alloy formation is clearly visible as a binding energy (BE) shift of both core levels Be 1*s* and W 4*f*, and in the valence band (VB) region. The surface alloy is stable and the remaining layer thickness is independent of the initial Be layer thickness. Using a combination of sputter depth profiling before and after annealing and Monte Carlo simulation of the sputter process (TRIDYN) the depth scale of Be–W inter-diffusion is determined.

Contents

[1] Author to whom any correspondence should be addressed.

PII: S1367-2630(06)23685-1

1. Introduction

Thin metal-on-metal films are investigated in terms of growth mechanism, electronic structure or material aspects [1]–[3]. Generally, photoelectron studies of the surface alloying process are of great interest since both core level and valence band (VB) spectra are sensitively affected by the alloying process. The core level shift was detected, with subsequent alloying e.g. in systems like $Cu_xPd_{(1-x)}$ and $Ag_xPd_{(1-x)}$ [4, 5] and was found to be dependent on the stoichiometric ratio of the respective metals.

The Be–W intermetallic system is of special interest due to the application of both metals as first wall materials in a fusion device [6]. Surface alloying and therefore changed material properties result from alloy formation because of the exposure of these materials to high heat and particle fluxes at the first wall of fusion devices. Due to the different electronic structures of the transition element tungsten (delocalized *d* electrons dominate) and beryllium (*s* states dominate) a strong influence of the alloying both on the core levels and the valence levels is expected though modifications in the coupling of the *d* states [4, 7]. This paper describes the first observation of a surface alloy in the Be–W system and the application of x-ray photoelectron spectroscopy (XPS) as a sensitive tool for a detection of the alloying process.

Two metals can either form an ordered or an unordered alloy depending on atomic radius, chemical behaviour and metal lattices. Be and W show neither comparable atomic radii, chemical behaviour, nor identical lattice structures. The earth alkaline metal beryllium has an atomic radius of 0.1113 nm and crystallizes in the hcp structure. Tungsten is a transition metal with a bcc bulk structure and an atomic radius of 0.1442 nm. The Be–W phase diagram exhibits three stoichiometric compounds: $Be_{22}W$, $Be_{12}W$ and Be_2W with small phase widths [8]. The respective intermetallic compounds are examples for ordered alloys. There also exists a miscibility gap in the phase diagram. We deposit Be films on polycrystalline tungsten. If a reaction occurs, we expect the formation of Be_2W, since we approach the Be_2W phase in the phase diagram from the W-rich side. First measurements of the Be–W intermetallic system were published by Watts [9]. In his study, Be and W were mixed as powders, pressed and subsequently annealed. Vasina and Panov [10] reported on the Be–W alloy formation using crystallographic measurements. We presented first results of thin Be films on tungsten and the formation of a beryllide at the PSI-16 conference [11]. Doerner *et al* observed the formation of a tungsten-beryllide in a beryllium-seeded deuterium plasma (PISCES-B) using Auger electron spectroscopy (AES) sputter depth profiles [12]. They also reported on the Be–W alloy formation, while operating a tungsten effusion cell filled with Be. The alloy formation was analysed by wavelength dispersive spectroscopy and scanning electron microscopy, respectively. Zuber *et al* [13] investigated Be films on W(110) and W(100) using work function change measurements ($\Delta\phi$), low energy electron diffraction (LEED) and electron energy loss spectroscopy (EELS). The substrates were held between 300 and 1000 K. Schlenk and Bauer [14] deposited Be on the W(110) surface at room temperature and characterized the system using AES, EELS, $\Delta\phi$ measurements, LEED and thermal desorption spectroscopy (TDS). They found a layer growth mode with a dense packing of Be in each layer. Chrzanowski and Bauer [15] reported on the adsorption of Be on W(211) using LEED, AES, EELS, TDS and $\Delta\phi$ measurements. The Be–W alloy formation was not addressed in these publications describing thin Be films on different W planes.

Johansson *et al* [16] measured surface core level shifts (SCLS) of Be single crystals using synchrotron radiation and compared these experimental data with calculated results reported by Aldén *et al* [17]. Synchrotron radiation promises the highest surface sensitivity by tuning

the photon energy such that small photoelectron kinetic energies are achieved. To study surface alloying, we are more interested in the surface-near region and interface. XPS measurements using Al Kα radiation are particularly suitable for these requirements since the photoelectron kinetic energy originating from Be 1*s* core levels is around 1370 eV. At these energies the inelastic mean free path of electrons is 1.4 nm, resulting in a surface near information depth. Therefore XPS analysis provides both, a high surface sensitivity, and information about chemical interactions in the near-surface region. Especially in the case of surface alloying XPS promises direct information about alloy formation in this intermetallic system.

2. Experimental procedure

The experiments are performed in a commercial ESCA spectrometer (PHI ESCA 5600). Using the monochromatic x-ray source (Al Kα, 1486.6 eV) the best spectral resolution is 0.26 eV. The analysed area is 0.8 mm in diameter. XPS measurements are performed under a take-off angle of 22° with respect to the surface normal. We refer the binding energy (BE) scale to the Au $4f_{7/2}$ signal at 84.0 eV and calibrate it additionally with the Cu $2p_{3/2}$ and Ag $3d_{5/2}$ signals [18]. During the experiments, the pressure is better than 2×10^{-8} Pa. The polycrystalline tungsten is cleaned using alternating sputter (3 keV, Ar^+) annealing (up to 970 K) cycles until no impurities are detected in XPS survey scans. The analysis system is connected to a preparation chamber where the Be layer deposition is performed using a commercial evaporator (Omicron, EFM3). The Be (HEK GmbH, 99.999%) is suspended in a BeO crucible. During the evaporation process, the pressure is better than 4×10^{-8} Pa. Despite the low pressure, the deposited Be layers contain small amounts of oxygen (see below). After room temperature deposition and analysis, the samples are annealed in steps of 100 K at 30 min per step up to 1070 K. Annealing at higher temperatures is not performed by now, since the expected operation temperatures at the first wall in a fusion device are around 1100 K at maximum. The XPS measurements are carried out after cooling down to room temperature. In additional long-term annealing experiments, XPS analysis is performed at the respective elevated temperature. The layers are analysed in high resolution spectra (pass energy 2.95 eV) in order to resolve spectral details. Survey scans (pass energy 93.90 eV) are used for the quantitative determination of film thicknesses. The Be films are analysed with both, survey and high resolution scans, after room temperature deposition, after each annealing step and while annealing, respectively. Details of the film thickness determinations using the XPS intensities from both substrate and film signals are given elsewhere [19]. We assume a layer growth mode after room temperature deposition and annealing experiments as reported in [14]. Since no densities for Be–W alloys are available, the layer thicknesses after annealing experiments given here are calculated using the density of metallic Be (1.85 g cm^{-3}). One monolayer Be is then equivalent to a thickness of 0.2 nm.

3. Results and discussion

3.1. Be layers after room temperature deposition

Figure 1 shows a sequence of high resolution spectra with increasing Be layer thicknesses. For the Be 1*s* spectra, a Shirley background is used, whereas from the W $4f$ signal a linear background is subtracted. Despite the low sensitivity due to the small photoionization cross-section, the Be 1*s*

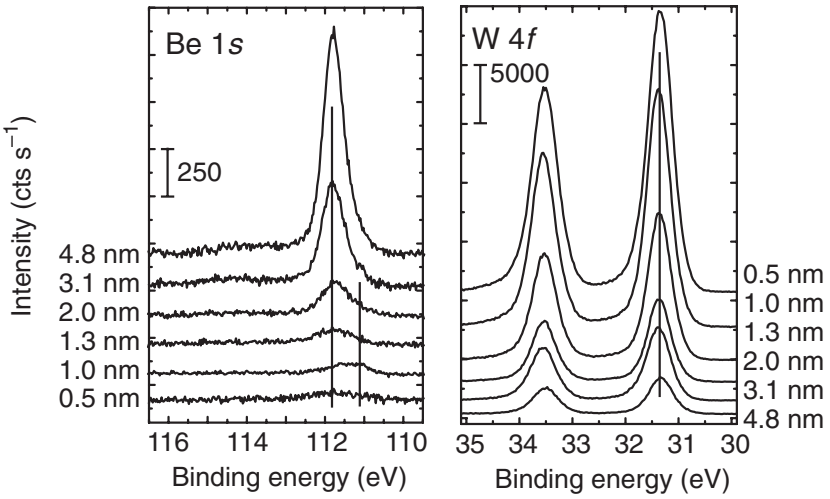

Figure 1. Be 1*s* and W 4*f* signals with increasing layer thicknesses after Be deposition at room temperature. The peak positions are marked at BEs of 111.8, 111.1 eV (Be 1*s*) and 31.4 eV (W 4*f*).

signals show a clearly visible fraction at lower BEs besides the metallic signal at 111.80 eV. As mentioned above, the layers are slightly contaminated with O and we find a small signal originating from BeO around 114.8 eV. The W 4*f* signals show no overall shift, but the full-width-at-half-maximum (FWHM) of the W $4f_{7/2}$ peak increases slightly (0.05–0.10 eV, at the detection limit!) compared to the clean substrate.

The Be 1*s* signals are fitted by Gauss–Lorentz curves [20][2] with a Gaussian ratio of 80% and with fixed BEs for metallic Be (111.8 eV) and oxidic Be (114.8 eV) [21, 22]. Both fractions, metallic and oxidic Be, are taken as reference points for the third component which is observed at 111.1 eV. In case of the W $4f_{7/2}$ signal, we position the metallic peak at 31.4 eV. The best agreement between data and fit curves is achieved using an additional peak at 31.0 eV. For the W 4*f* signals, we employ asymmetric Doniach–Šunjić functions [23] and keep the 7/2 and 5/2 spin–orbit splitting and area ratio constant at $\Delta = 2.18$ eV and 0.77, respectively. We assign the components at lower BEs in both the Be 1*s* and W 4*f* signals to a Be–W surface alloy. SCLS on clean Be substrates are in the same range (first layer: −0.82 eV, second layer: −0.57 eV, third layer: −0.26 eV [16]). However, using Al Kα radiation, we are sensitive for the whole near-surface region (several nanometres) and surface core levels can be excluded as origin of the additional peak in the Be 1*s* signal. To detect SCLS, the photoelectron kinetic energy must be close to the minimum of the electron escape depth. This is achieved by a photon energy around 135 eV, available at a synchrotron [16]. Using Al Kα radiation, however, we are not sensitive for SCLS and cannot resolve these BE shifts characteristic for the first atomic layers of a solid. Furthermore, we determine an additional signal in the W 4*f* signal by applying the peak fitting procedure, which cannot be explained by a SCLS within the W substrate signal. The alloy intensity in the Be 1*s* signal increases up to a deposition of ∼4 ML (∼0.8 nm) and is accompanied by a maximum in FWHM. In this film thickness region, the alloy contribution to the Be 1*s* intensity is ∼50%. Further Be deposition leads to an increase in metallic Be intensity accompanied by a decrease in alloy intensity (see also [11]). This indicates that the Be–W alloy phase is only present at the

[2] This code uses a sum of Gauss and Lorentz functions to approximate the Voigt function.

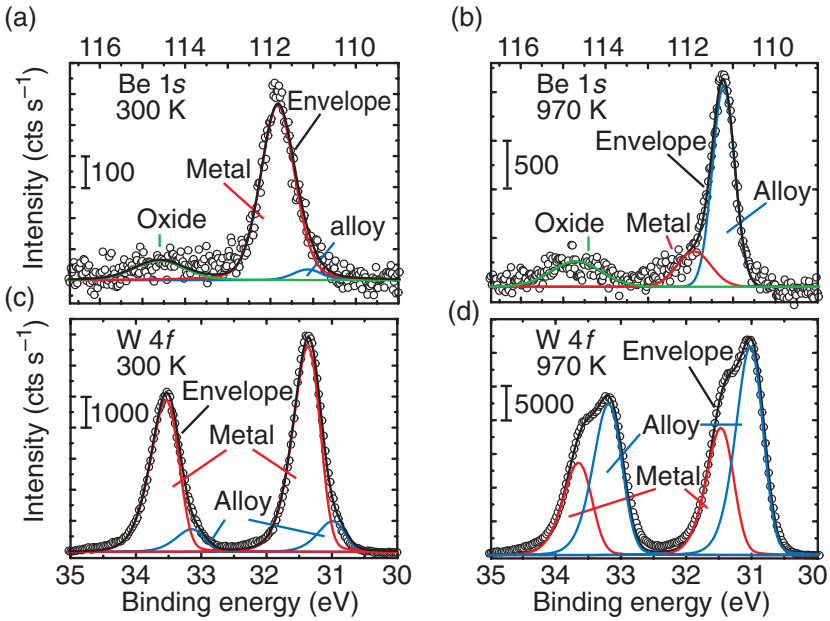

Figure 2. Be 1*s* and W 4*f* signals of a 2 nm Be film on W after room temperature deposition (panels (a) and (c)) and annealing at 970 K (panels (b) and (d)). The metal and alloy components (and the oxide in the Be 1*s* signals) are identified by fitting peaks representing metallic and alloy components to the data. Raw data are plotted as circles, the black line represents the sum of the fit functions.

interface between substrate and Be layer, since additionally deposited Be attenuates the alloy signal from the buried interface. The oxide concentration is nearly constant throughout the Be thickness series (∼10%), therefore the BeO is equally distributed in the whole Be layer. The alloy intensity in the W 4*f* signal amounts to 10 at-% at maximum. No additional components are identified besides metal and alloy. In particular, no oxide component or broadening due to a W–O surface layer [24][3] is observed. In that case even a submonolayer coverage would lead to a broadening or additional signal.

The VB spectra are dominated by the W substrate. A sharp feature at ∼2.3 eV and a broader signal around 5 eV are observed in good agreement with bulk W spectra [25]. A broad signal around 8 eV appears in XPS measurements of a clean Be substrate [26], which is not observed here. We also do not identify a O 2*p* signal (6–7 eV).

3.2. Annealing experiments

The peak fitting procedure as described and applied above becomes more evident when applied to the annealing experiments. Figure 2 shows Be 1*s* and W 4*f* signals measured at a 2 nm Be film on W after deposition at 300 K and after annealing to 970 K (remaining thickness 1.2 nm). From the raw data, a background is subtracted and peaks representing the elemental, alloy and oxide components are fitted (as described above, subsection 3.1). Whereas after 300 K deposition

[3] In separate measurements we adsorbed O_2 and atomic O on W_{poly}. In this case, the formation of a W–O first layer is clearly seen in a broadening of the W 4$f_{7/2}$ peak by 0.11 eV and in the appearance of intensity at the O 2*p* position at a BE of 6–7 eV, in accordance with this reference.

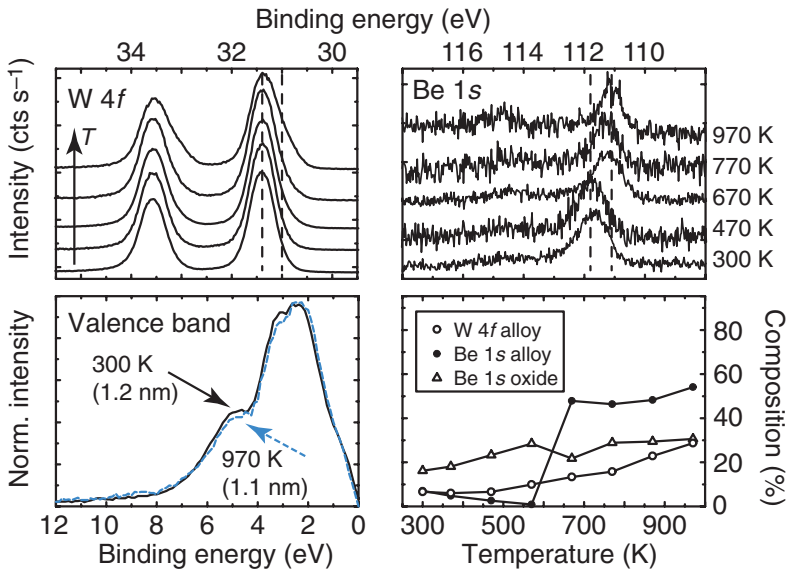

Figure 3. Be 1*s*, W 4*f* signals and the VB region of a 1.2 nm Be film, after the indicated annealing steps. In the Be 1*s* signal, a shift to the alloy position occurs at 670 K, whereas the changes in the W 4*f* peaks are gradual.

(spectra shown in panels (a) and (c) for Be 1*s* and W 4*f*, respectively) the necessity of the alloy peaks can still be challenged, it is obvious for the signals measured after the 970 K annealing step (see panels (b) and (d) for Be and W). When applying the fit parameters from the high-temperature step to the 300 K spectra, the data analysis becomes consistent in the whole temperature range. The Be 1*s* signal can be deconvoluted into a peak representing BeO, and peaks for Be in the metallic and in the alloy state. In the W 4*f* signal, two doublets are necessary to represent the experimental data which are assigned to W metal and W in a Be–W alloy.

The behaviour of the Be films upon annealing depends on the initial film thickness. Figure 3 summarizes the evolution of a Be layer with an initial film thickness of 1.2 nm (∼6 ML) with increasing annealing temperatures. The overall thickness of the Be layer decreases only marginally during the annealing series and amounts to 1.1 nm after 970 K. The signals in the Be 1*s*, W 4*f* and VB photoelectron energy regions are unchanged after 300 K deposition and annealing steps below 670 K. Above this temperature, a pronounced increase in the alloy fraction is observed in the Be 1*s* signal. After the final annealing step at 970 K, we determine 54% alloy and 31% oxidic fraction, respectively, in the Be 1*s* signal by applying the peak fitting procedure. 15% of the Be 1*s* signal are still in the metallic state. Due to the small layer thickness and the contribution of the substrate, the W 4*f* signal does not show an abrupt increase in the alloy component. However, the reaction between Be and W is unambiguously visible in a broadening towards lower BEs and finally leads to a shoulder after 970 K. After this annealing step, we examine 29% signal intensity originating from the alloy fraction within the W 4*f* signal. The residual signal intensity (71%) is in the metallic state. Additionally a small shift of 0.15 eV to lower BEs is noticeable in the VB.

In contrast to the almost unchanged Be thickness in this film, the Be intensity starts to decrease at 670 K in an annealing series starting with a 3.3 nm Be film. The results for this thick film are shown in figure 4. After the final annealing step at 1070 K, the residual film thickness

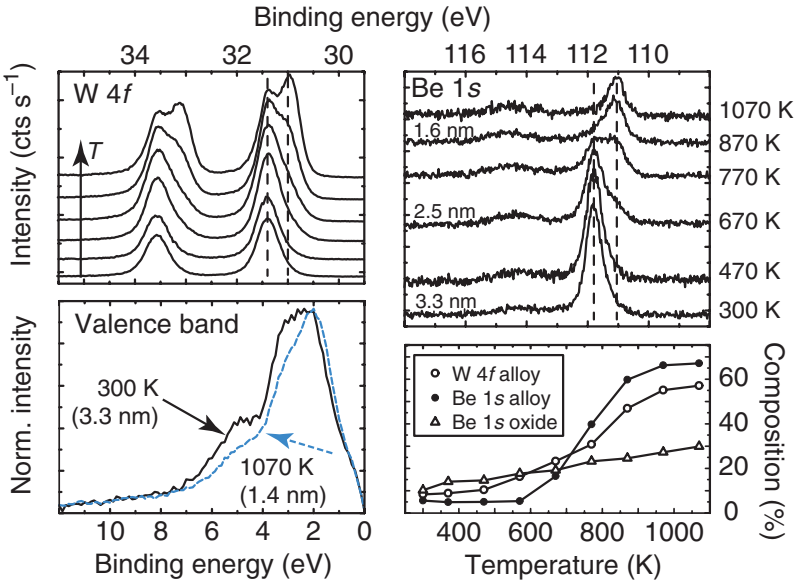

Figure 4. Thermal behaviour of a 3.3 nm thick film. The alloying reaction is clearly visible in all measured signals. In agreement with the Be film shown in figure 3 the alloy fraction increases above 670 K, accompanied by a decrease in film thickness.

amounts to 1.4 nm, which is clearly thinner than the initial film. All recorded XPS signals (Be 1*s*, W 4*f*, VB) unambiguously prove the alloy formation. After 1070 K, the Be 1*s* signal of the thick film is composed of about 67% alloy, 30% BeO and the remaining 3% are still in the metallic state. The appearance of the alloy peak in the W 4*f* signal is more pronounced than for the thin film: a second peak evolves which after 1070 K annealing is stronger than the metallic peak. We determine 57% alloy and 43% metal fraction intensity, respectively, within the W 4*f* signal. Also more pronounced are the changes in the VB region: the broad feature between 1 and 4 eV—characteristic for the tungsten *d* band—develops a maximum at 2 eV. The FWHM of this band decreases from 2.8 eV at 300 K to 2.6 eV after 1070 K. In the case of the 3.3 nm film, the band shift amounts to 0.15–0.20 eV, as determined from the low BE side of the VB spectra in figure 4.

The surface alloying between Be and W is further analysed in long-term annealing experiments, shown in figure 5. Be layers with increasing thicknesses are annealed at 770, 870 and 970 K, holding the samples at these elevated temperatures for several hours, without cooling to room temperature for XPS analysis. Due to the low sensitivity for the Be 1*s* signal exclusively, the W 4*f* signal is analysed in the high resolution mode. Spectra in survey resolution (for film thickness determination) and high resolution (W 4*f* for chemical analysis) are performed alternatingly. The decrease in film thickness (see table in figure 5) occurs already almost completely within the ramp-up time to the respective temperatures (10–13 min for 770–970 K). Immediately after reaching the annealing temperatures, the calculated Be thicknesses are between 1.0 and 1.2 nm. The film thickness then stays constant at these values. The remaining Be thickness in these experiments is comparable to that observed for the thin Be layer, shown in figure 3. The alloy intensity within the W 4*f* signal increases with temperature and changes then only marginally with annealing time. After the annealing experiments, the relative alloy concentrations

T (K)	770	870	970
d_{Be} (nm) at 300 K	1.3	1.5	2.0
d_{Be} (nm) at T	1.0	1.2	1.2
Alloy W 4f (%)	15	30	55

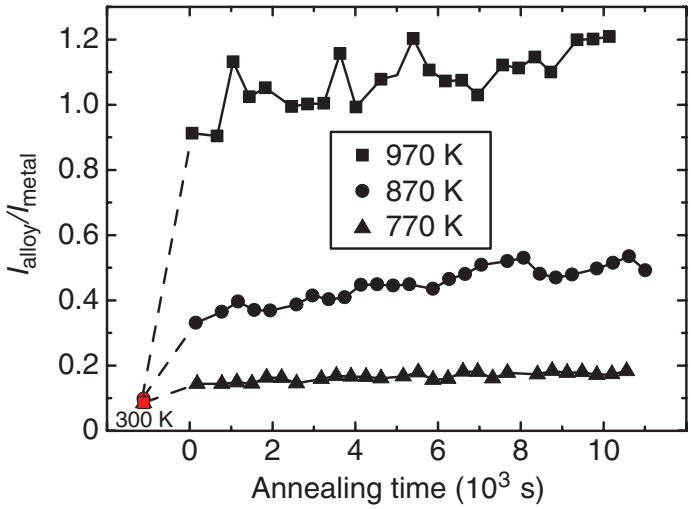

Figure 5. Ratio of alloy and metal intensities within the W 4f signals. The samples were held at the given elevated temperatures. The first data points indicate the intensity ratio after Be deposition at 300 K. The following data points are measured at elevated temperatures. Estimated layer thicknesses after room temperature deposition, while annealing and the relative alloy amount within the W 4f signal after annealing, respectively, are given in the table.

are determined from the W 4f signal (see table in figure 5). The absolute alloy amounts show also a clear tendency with a stoichiometric ratio representing Be_2W at 970 K.

3.3. Discussion

The XPS analysis of thin Be films on W indicates the formation of a surface alloy even after room temperature deposition. Both core levels show an additional signal intensity originating from the Be–W alloy. Since the VB spectra are not affected by this compound, the formation of a surface alloy is proved.

The survey scans after room temperature deposition are further analysed by comparing the inelastic background region around the W 4d signal. Tougaard reported on the influence of the surface morphology on the inelastic background in XPS spectra [27, 28]. An analysis of the background region around the W 4d signal in XPS spectra of Be films on W indicates a layer growth mode. This result in combination with measurements given in [14] justifies the determination of layer thicknesses with the assumption of layer-by-layer growth mode. The same procedure is used for the analysis of the surface morphology of Be films on W after thermal treatment. From the survey scans in both experimental procedures (temperature steps and long-term annealing) again an island formation is excluded which permits the film thickness estimation as mentioned above.

The thermal behaviour of thin Be films on W depends on the initially deposited layer thickness. In annealing experiments starting with different Be thicknesses, three coverage regions

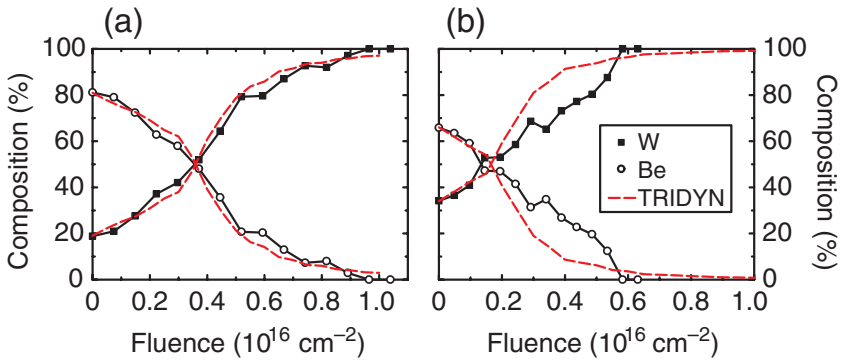

Figure 6. Comparison of the measured depth profiles of an untreated (a) and an annealed Be film (b), respectively, with TRIDYN results. The deposited film thickness is 1.9 nm (a), whereas the residual film after annealing at 970 K amounts to 1.2 nm (b).

can be distinguished: (i) $d_{Be} < 1.4$ nm, (ii) $d_{Be} = 1.4$–3.0 nm and (iii) $d_{Be} > 3.0$ nm. In region (i), the film thickness is not affected by annealing up to 970 K. Above 670 K, alloying sets in. The formed alloy is stable during further annealing and at 970 K, a Be_2W stoichiometry is measured. In XPS measurements, an overestimation of the W substrate is observed making the evaluation of the stoichiometric ratio within the alloy compound difficult. However, the absolute alloy amounts indicate a ratio of Be : W of $\sim 2 : 1$ at 970 K rather than $Be_{12}W$ or $Be_{22}W$. In region (ii), the layer thickness decreases very fast and already within the temperature ramp-up time at the long-term annealing runs. The remaining layer thickness is 1.0 to 1.2 nm, both at elevated temperatures and after cooling to 300 K. The final alloy thickness is therefore comparable to the alloy thickness observed for region (i). Finally, region (iii) is characterized by a very slow decrease in Be thickness, starting at 670 K. For initial Be thicknesses above 3 nm, a Be thickness of >1.4 nm remains at 970 K. As in the two other regions, also a stable intermixing zone is observed.

In order to clarify whether Be diffusion or desorption leads to the observed decrease in film thickness in region (ii), sputter depth profiles are measured after the annealing experiments (3 keV Ar^+, 45° incidence). They are compared to a depth profile of a deposited Be layer (1.9 nm) without annealing. The ion–surface interactions are simulated using TRIDYN. This code accounts for kinematic collisional processes and adapts the sample composition dynamically [29]. Figure 6 compares the as-deposited case in (a) with an annealed film (thickness 1.2 nm after 970 K), shown in panel (b). The oxygen contamination is not considered here. The agreement between measured depth profile and TRIDYN simulation in (a) is very good and justifies again the assumption of a Be layer morphology. The apparent broadening of the film–substrate interface is an artefact due to ion-beam induced mixing and is well reproduced by the simulation [30]. In (b) a small deviation between the measured profile and the TRIDYN result is visible. The alloy formation leads to an intermixing within a restricted range. However, if diffusion of Be into the W substrate were the reason for the Be loss from the XPS analysis depth, Be intensity was to be found in greater depths than actually measured. Since the Be 1*s* signal vanishes for Ar^+ fluences above 6×10^{15} cm^{-2}, Be diffusion into the W bulk is excluded as reason for the Be losses from the surface. The only possible loss channel therefore is Be desorption.

The results presented here demonstrate for the first time the formation of a Be–W surface alloy during annealing of thin Be films on W. The alloy formation is verified in shifts both

Table 1. BEs used and determined (Be_2W alloy) in this work.

Core level	Chemical state	E_B(eV)
Be 1s	Metal	111.8
	Alloy (Be_2W)	111.1
	Oxide (BeO)	114.8
W 4$f_{7/2}$	Metal	31.4
	Alloy (Be_2W)	31.0

in the core level and the valence level BEs. The core level shifts are independent on the stoichiometry and amount to −0.7 eV (Be 1s) and −0.4 eV (W 4$f_{7/2}$), as compared to the respective metal values (see table 1). This is a clear indication for the formation of an ordered alloy with a fixed stoichiometry (Be_2W) as expected for the Be–W system. Random alloys or different stoichiometries ($Be_{12}W$, $Be_{22}W$) would lead to a continuous peak shift or additional signal intensities, respectively, in both core levels. Measurements of a W film (200 nm) on polycrystalline Be prove this result. In these measurements, we observe a formation of $Be_{12}W$ using a combination of RBS (Rutherford backscattering spectroscopy) and XPS [31]. The BE shift of that alloy compound within the Be 1s signal amounts to −0.5 eV, which is smaller than the result given above. Since the BE shift for thin Be films on W is constant within the Be 1s and W 4f signals after room temperature deposition and annealing experiments, respectively, the formation of a surface alloy is proved. The structure of this surface alloy has to be analysed with other techniques. The VB modifications are in accordance with calculations for other d band metals [7]. In addition to the core level shifts, the formation of a Be–W surface alloy is also detected by VB photoemission spectroscopy showing a reduced d band coupling due to the alloying of tungsten with the s metal beryllium. This behaviour is a clear indicator for a decreased d band coupling caused by the screening of the d orbitals by the Be s states [7]. Since coupling of d orbitals is best between alike atoms, the reduction of the d band width concludes the intermixing of Be and W atoms. This leads to a stronger localization of the W d states and to narrowing of the d band. This effect should be even more pronounced when the foreign atomic species is an s metal. The tendency to preserve the d band filling then leads to the shift which is observed experimentally.

4. Summary

Small alloy intensities are detected already after Be deposition on W at 300 K and increase significantly above 670 K. The onset of alloy formation is independent of the initial film thickness. In long-term annealing experiments, the alloy amount and reaction rate, respectively, do not further increase with annealing time. The alloy formation is limited to a thin layer of 1.0 to 1.2 nm. This observed intermixing layer thickness is comparable for all Be films described here. Additional metallic Be not incorporated in the alloy is desorbed from the surface rather than dissolved in the W substrate at elevated temperatures.

References

[1] Kolodziej J J, Madey T E, Keister J W and Rowe J E 2002 *Phys. Rev.* B **65** 075413
[2] Thayer G E, Ozolins V, Schmid A K, Bartelt N C, Asta M, Hoyt J J, Chiang S and Hwang R Q 2001 *Phys. Rev. Lett.* **86** 660
[3] Bischoff M M J, Yamada T, Quinn A J, van der Kraan R G P and van Kempen H 2001 *Phys. Rev. Lett.* **87** 246102
[4] Mårtensson N, Nyholm R, Calén H, Hedman J and Johansson B 1981 *Phys. Rev.* B **24** 1725
[5] Olovsson W, Abrikosov I A and Johansson B 2002 *J. Electron Spectrosc. Relat. Phenom.* **127** 65
Olovsson W, Abrikosov I A and Johansson B 2003 *J. Electron Spectrosc. Relat. Phenom.* **129** 81 (erratum)
[6] Parker R R 2000 *Nucl. Fusion* **40** 473
[7] Ganduglia-Pirovano M V, Kudrnovský J and Scheffler M 1997 *Phys. Rev. Lett.* **78** 1807
[8] Massalski T B, Okamoto H, Subramanian P R and Kacprzak L 1996 *Binary Alloy Phase Diagrams* 2nd edn (Materials Park, OH: ASM International)
[9] Watts C R 1968 *Int. J. Powder Metall.* **4** 49
[10] Vasina E A and Panov A S 1974 *Metally* **1** 197
[11] Wiltner A and Linsmeier Ch 2005 *J. Nucl. Mater.* **337–339** 951
[12] Doerner R P, Baldwin M J and Causey R A 2005 *J. Nucl. Mater.* **342** 63
[13] Zuber S, Sidorski Z and Polański J 1979 *Surf. Sci.* **87** 375
[14] Schlenk W and Bauer E 1980 *Surf. Sci.* **94** 528
[15] Chrzanowski E and Bauer E 1986 *Surf. Sci.* **173** 106
[16] Johansson L I, Johansson H I P, Andersen J N, Lundgren E and Nyholm R 1993 *Phys. Rev. Lett.* **71** 2453
[17] Aldén M, Skriver H L and Johansson B 1993 *Phys. Rev. Lett.* **71** 2457
[18] Seah M P, Gilmore I S and Beamson G 1998 *Surf. Interface Anal.* **26** 642
[19] Wiltner A and Linsmeier Ch 2004 *Phys. Status Solidi* a **201** 881
[20] MultiPak, Ver. 6.1A, Physical Electronics 1999
[21] Goldstraß P and Linsmeier Ch 2000 *Nucl. Instrum. Methods* B **161–163** 411
[22] Linsmeier Ch and Wanner J 2000 *Surf. Sci.* **454–456** 305
[23] Doniach S and Šunjić M 1970 *J. Phys. C: Solid State Phys.* **3** 285
[24] Riffe D M and Wertheim G K 1998 *Surf. Sci.* **399** 248
[25] Moslemzadeh N, Barrett S D, Dhanak V R and Miller G 2003 *J. Electron Spectrosc. Relat. Phenom.* **130** 119
[26] Hüfner S 1995 *Photoelectron Spectroscopy* (Berlin: Springer)
[27] Tougaard S 1996 *J. Vac. Sci. Technol.* A **14** 1415
[28] Tougaard S 1998 *Surf. Interface Anal.* **26** 249
[29] Eckstein W 1991 *Computer Simulation of Ion–Solid Interactions* (Berlin: Springer)
[30] Schmid K, Wiltner A and Linsmeier Ch 2004 *Nucl. Instrum. Methods Phys. Res.* B **219–220** 947
[31] Linsmeier Ch, Ertl K, Roth J, Wiltner A, Schmid K, Kost F, Bhattacharyya S R, Baldwin M and Doerner R P 2006 *J. Nucl. Mater.* at press